Ain Shams Engineering Journal 15 (2024) 102506

Contents lists available at ScienceDirect

Ain Shams Engineering Journal

journal homepage: www.sciencedirect.com

Investigating the effect of the absence and presence of a mask with different porosities on the absorption of particulate matter by the human respiratory system using computational fluid dynamics

Ashkan Abbasi Tadi [a], Dheyaa J. Jasim [b], As'ad Alizadeh [c], Navid Nasajpour-Esfahani [d], Mahmoud Shamsborhan [e], Maboud Hekmatifar [f,*]

[a] Department of Mechanical Engineering, Khomeinishahr Branch, Islamic Azad University, Khomeinishahr, Iran
[b] Department of Petroleum Engineering, Al-Amarah University College, Maysan, Iraq
[c] Department of Civil Engineering, College of Engineering, Cihan University-Erbil, Erbil, Iraq
[d] Department of Material Science and Engineering, Georgia Institute of Technology, Atlanta, GA 30332, USA
[e] Department of Mechanical Engineering, College of Engineering, University of Zakho, Zakho, Iraq
[f] Department of Mechanical Engineering, Islamic Azad University, Iran

ARTICLE INFO

Keywords:
Computational fluid dynamics (CFD) simulation
Respiratory system
Particulate matter
Filtration

ABSTRACT

Particulate matter (PM) with a diameter of less than 10 μm is among the pollutants in cities that can be inhaled by humans. They are 100 μm in size and are neutralized by the lungs' cleaning system. Particles with a size of 2.5 μm cause cardiac and pulmonary discomfort by settling in the respiratory system. In this research, the absorption of PM by the respiratory system simulated with CFD has been investigated. Also, the effect of using a mask with a porosity of 0.07 and 0.2 on the absorption of PM has been investigated. The results show that the percentage of particle absorption for laminar flow and flow rates of 20, 25, and 30 lit/min is equal to 96.87 %, 97.19 %, and 97.64 %. With the increase of fluorite, the percentage of absorption of particles also increases. The percentage of particle absorption for turbulent flow and flow rates of 40, 60, and 100 lit/min is equal to 98.67 %, 98.65 %, and 99.59 %. With the increase of fluorite, the percentage of absorption of particles also increases. The absorption of particles for 1, 2.5, and 10 μm is close to each other for laminar respiratory flows, while it does not show this in a turbulent flow. The respiratory filter with a porosity of 0.07 is ideal and can filter particles up to 99 %. According to the results obtained in this project, in the porosity of 0.07, the filtration of 1-μm particles is the best compared to the rest of the investigated porosity.

1. Introduction

Air pollution refers to the presence of harmful substances in the air that can have negative effects on human health, the environment, and the climate. These substances can include gases, such as carbon monoxide, sulfur dioxide, nitrogen oxides, and ozone, as well as PM, such as dust, smoke, and soot [1,2]. Sources of air pollution can include natural phenomena like wildfires and volcanic activity, as well as human activities such as transportation, industrial processes, and energy production. Exposure to air pollution has been linked to a range of health problems, including respiratory diseases, heart disease, stroke, and cancer. Efforts to reduce air pollution can include improving fuel efficiency in vehicles, promoting the use of clean energy sources, and implementing regulations on industrial emissions. Personal actions, such as reducing vehicle use and using public transportation or biking instead, can also help to reduce individual contributions to air pollution [3]. The presence of PM in the air, also known as PM, can have significant health and environmental impacts. PM can come from a variety of sources, including combustion processes (such as the burning of fossil fuels), industrial processes, agricultural activities, and natural sources such as dust and wildfires [4,5]. PM can be divided into different categories based on their size, with smaller particles generally being more harmful to human health. The smallest particles, known as fine $PM_{2.5}$, are less than 2.5 μm in diameter and can penetrate deep into the lungs and even enter the bloodstream. Coarse PM_{10}, which is between 2.5 and 10 μm in diameter, can also cause respiratory problems [6,7]. Exposure

* Corresponding author.
E-mail address: maboud.hekmatifar@iaukhsh.ac.ir (M. Hekmatifar).

https://doi.org/10.1016/j.asej.2023.102506
Received 9 July 2023; Accepted 7 September 2023
Available online 5 October 2023
2090-4479/© 2023 THE AUTHORS. Published by Elsevier BV on behalf of Faculty of Engineering, Ain Shams University. This is an open access article under the CC BY-NC-ND license (http://creativecommons.org/licenses/by-nc-nd/4.0/).

to PM has been linked to a range of health problems, including respiratory, cardiovascular, cancer, neurological, and reproductive problems [8,9]. In addition to its health impacts, PM can also have environmental impacts. It can contribute to the formation of acid rain, damage crops, and forests, and reduce visibility [10]. Efforts to reduce PM pollution can include improving fuel efficiency in vehicles, promoting the use of clean energy sources, and implementing regulations on industrial emissions. Personal actions, such as reducing vehicle use and using public transportation or biking instead, can also help to reduce individual contributions to PM pollution [11]. Kim et al. [12] investigated the improvement of Filter performance to remove indoor air pollution by CFD simulation. The results show that when applying the sub-filter and the Coanda effect at the same time, it was confirmed that the sub-filter was more efficient than the Coanda effect. Nie et al. [13] investigated the multi-factor ventilation parameters for reducing energy air pollution in coal mines. The results show that, $Q_c = 150$ m^3/min, $Q_e = 250$ m^3/min. According to the results of the field experiments, the diffusion distance of the highly concentrated dust L_H is reduced to 9.3 m, and the diffusion distance of the low-concentrated dust L_L is reduced to 36.3 m, which effectively improves the air quality during coal energy mining. Meesang et al. [14] investigated the modeling of the feasibility of air pollution treatment using plants as filters by CFD simulation. The results showed that the average airflow velocity (top view/front view) was 0.23/0.27, 0.57/0.43, 0.71/0.80, and 0.97/0.96 m/s, respectively. At all velocities of inlet air, airflow passed through all locations and contacted the surfaces of every panel. McNabola et al. [15] investigated the Measurement and prediction of air pollution on the boardwalk in Dublin, Ireland. The results of the study show significant reductions in pedestrian exposure to both traffic-derived particulates and hydrocarbons along the boardwalk as opposed to the footpath. In this study, particles with a diameter of 1, 2.5, and 10 μm enter the respiratory system, and the pattern and extent of their absorption in the respiratory system are checked. Then the mentioned particles in laminar flow rates of 20, 25, and 30 lit/min and turbulent flow rates of 40, 60, and 100 lit/min without the presence of a respiratory filter and once considered at the beginning of air entering the nose through the left nasal passage. They will enter the respiratory system. Finally, the results obtained from solving the flow in the respiratory system with the presence of particles before and after the existence of the respiratory filter are checked and the amount of difference in the settling of particles in different parts of the respiratory system in the laminar and turbulent flow and the acceptable effect of the respiratory filter are determined.

2. Governing equations

In this research, the flow field was simulated in resting, sitting, and standing states. Despite the geometrical complexity of the respiratory tracts, according to the experimental results, the flow regime is turbulent and steady state. Also, since the fluid pressure drop is low along the path, the air density is considered constant in this simulation. The main equations include the continuity equation, and momentum equation [16]:

Continuity equation

$$\nabla.(\rho v) = 0 \tag{1}$$

Momentum equation:

$$\frac{\partial}{\partial x_i}(\rho u_i u_j) = -\frac{\partial P}{\partial x_j} + \frac{\partial}{\rho x_i}\left[\mu\left(\frac{\partial u_i}{\partial x_j} - \overline{\rho u_i' u_j'}\right)\right] \tag{2}$$

The Reynolds stresses, mentioned in Eq. (2), are discretized by Boussinesq's hypothesis as follows:

$$-\overline{\rho u_i' u_j'} = \mu_t\left(\frac{\partial u_i}{\partial x_j} + \frac{\partial u_j}{\partial x_i}\right) - \frac{2}{3}(\rho k)\delta_{ij} \tag{3}$$

μ_t is the turbulent viscosity of the fluid, while δ_{ij} is the Kronecker delta.

Turbulence modeling is a key issue in most CFD simulations. Turbulence modeling is a field within CFD that aims to analyze the properties of turbulent flows [21–23].

In this study, the turbulence phenomenon is performed using Realizable k-ε model. This model was improved in response to the shortcomings of the classical k-ε model and utilized the same kinetic energy equation as before, but the ε equation is diverse:

Transport Equations:

$$\begin{gathered}\frac{\partial}{\partial x_j}(\rho \varepsilon u_j) = \frac{\partial}{\partial x_j}\left[\left(\mu + \frac{\mu_t}{\sigma_\varepsilon}\right)\frac{\partial \varepsilon}{\partial x_j}\right] + \rho C_1 S\varepsilon - \rho C_2\frac{\varepsilon^2}{k + \sqrt{\nu\varepsilon}} + C_{1\varepsilon}\frac{\varepsilon}{k}C_{3\varepsilon}P_b + S_\varepsilon \\ \frac{\partial}{\partial x_j}(\rho k u_j) = \frac{\partial}{\partial x_j}\left[\left(\mu + \frac{\mu_t}{\sigma_k}\right)\frac{\partial k}{\partial x_j}\right] + P_k + P_b - \rho\varepsilon - Y_M + S_k\end{gathered} \tag{4}$$

$$C_{1\varepsilon} = 1.44, C_{2\varepsilon} = 1.92, C_\mu = 0.09, \sigma_k = 1.0, \sigma_\varepsilon = 1.$$

$$C_1 = \max\left[0.43, \frac{\eta}{\eta + 5}\right], \quad \eta = S\frac{k}{\varepsilon}, \quad S = \sqrt{2S_{ij}S_{ij}}\ , \quad S_{ij} = \frac{1}{2}\left(\frac{\partial u_i}{\partial x_i} + \frac{\partial u_j}{\partial x_i}\right), \quad C_2 = 1.9 \tag{5}$$

Wherein the values of the σ_k and σ_ε are similar to the standard k-ε model.

Turbulence viscosity:

$$\mu_t = \rho C_\mu \frac{k^2}{\varepsilon}, \quad C_\mu = \frac{1}{A_0 + A_s\frac{kU^*}{\varepsilon}} \tag{6}$$

C_μ is a variable proposed by Reynolds. A_0, A_s, and U^* constants can be found in the Fluent software user help. To check the amount of pressure drop from the nose inlet to its end, the dimension cessation of the pressure values is needed, which is achieved by Eq. (7).

$$C_p = \frac{\Delta P}{\frac{1}{2}\rho u^2} \tag{7}$$

ΔP is the pressure drop, ρ is the density and u is the inlet velocity.

In this work, Ansys Fluent software is used to solve the flow field. This software converts the governing equations into algebraic equations using the finite volume method so that they can be solved by numerical methods. To couple the velocity and pressure fields in steady-state calculations, the SIMPLE algorithm is usually used. The SIMPLE algorithm is used for the coupling between the velocity and pressure fields in the present work [17]. The Lagrangian point of view was used to investigate the movement and settling rate of particles. In this view, the movement of each particle is investigated independently in the flow field. As mentioned before, the concentration of PM in inhaled air is very low, so the one-way interaction method is used to investigate the behavior of particles; That is, only the particles are affected by the characteristics of the flow and the effect of the particles on the behavior of the flow is ignored. Also, the mutual influence of particles on each other, which is caused by their collision and reflection or adhesion, has been ignored. Particles gain speed and acceleration under the influence of the flow field, and the main form of their spreading and settling is inertial force. Particles move in a certain direction in the flow field. With a sudden change in the flow direction, the particles remain in the original direction due to their inertia and cannot follow their original flow path and cut off their asymptotic flow paths. In this process, particles may hit the wall and settle on the surface of the wall before taking on the flow behavior again. Considering that fluid drag and particle weight force are effective forces on movement, therefore, the equation of spreading particles with macro dimensions can be presented as follows[18,19]:

$$\frac{du_i^p}{dt} = \frac{3\mu C_{DP} Re_p}{4\rho_p d_p^2}\left(\vec{u}_i - \vec{u}_i^p\right) + g \tag{8}$$

ρ_p is the particle density, $\vec{u}_i^p$ is the particle velocity, $\vec{u}_i$ is the velocity of the fluid phase, g is the gravity of the earth, and Re_p is the relative Reynolds number of the particle, which is defined as follows [18,19]:

$$Re_p = \rho\left|\vec{u}_j - \vec{u}_j^p\right| \times \frac{d}{\mu} \tag{9}$$

where d is the aerodynamic diameter of the particle.

$$C_{DP} = \frac{C_D}{C_{slip}} \tag{10}$$

The C_D is the particle drag coefficient and C_{slip} is the Cunningham slip correction factor, which are defined as follows:

$$C_D = \frac{24}{Re_p}\left(1 + 0.15Re_p^{0.687}\right) \tag{11}$$

$$C_{slip} = 1 + \frac{2\lambda}{d_p}\left[1.257 + 0.4e^{-1.1\frac{d_p}{2\lambda}}\right] \tag{12}$$

λ is the distance between air molecules is about 0.07 μm at T = 25 °C. The aerodynamic diameter of the particle is equivalent to the particle diameter of a sphere with a standard density that has a static velocity equal to the static velocity of the investigated particle, and is calculated from the Eq. (13) [18,19]:

$$V_{TS} = \frac{\rho_0 d_a^2 g}{18\mu} \tag{13}$$

ρ_0 is the standard density, μ is the air viscosity and V_{TS} is the stopping velocity of the particle. The particles entered with the solution domain, after tracking, will be in one of the following states:

- They hit the walls of the duct (reflect).
- They escape without hitting the walls.
- They remain in the part of the solution domain (incomplete).
- They are attracted to the walls (trap).

3. Assumptions and boundary conditions

Air with a dynamic viscosity of 1.7894×10^5 kg/m.s and a density of 1.225 kg/m^3 is considered a continuous medium. According to the area of the entrance surface, the entrance velocity in the left and right channels is 3.5 and 3.19 m/s, respectively. The flow rate for the nose at the entrance of the left and right channels is considered equal. Since the concentration of PM in inhaled air is very low, it can be assumed that only the flow field affects the diffusion of PM, and particles do not have much effect on the flow field, and therefore, to track particles in the flow field, one-way interaction method is used. is used In this way, first the flow field is simulated, and then micrometer-sized particles are sprayed in this field.

4. Geometric models

To reconstruct the real geometry of the respiratory tract, in the first step, medical images of this organ should be prepared. In this study, a 24-year-old man in Al-Zahra Hospital (Isfahan, Iran), was imaged from the nasal and oral respiratory tracts to the tracheal outlet using the X-ray method using a Multi-Slice CT scan machine. The cross sections used for volume generation were imaged with 0.49 mm cutting distances and 120 kVp power and 100 mA. These images were checked by a radiologist as well as an otolaryngologist and the health of the respiratory tract was confirmed. In this project, Mimics software is used to extract geometric models from CT scan images. Fig. 1 shows the coronal, sagittal, and axial views of the patient's CT scan images extracted from CT scan images using Mimics software. As you can see in Fig. 1, the complete geometry of the nose up to the end of the trachea is extracted from CT scan images using Mimics software. In this figure, the upper right image is axial, the upper left is sagittal, and the lower left is coronal. As it is known, the spaces related to the respiratory passages are separated from the rest of the spaces with blue color.

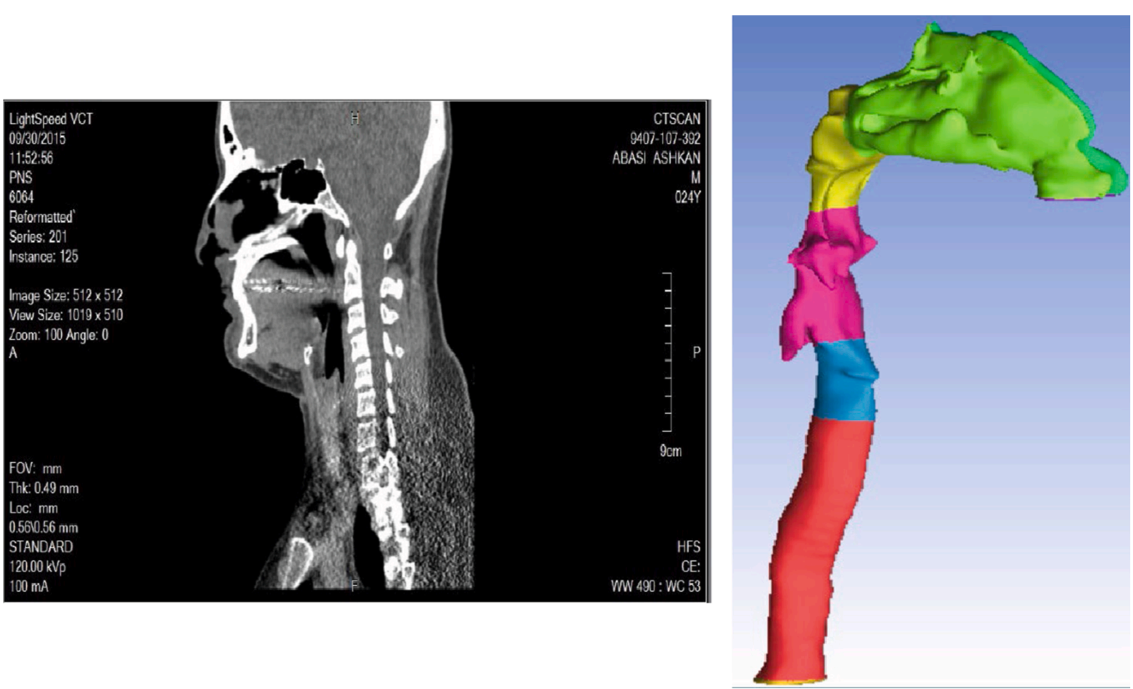

Fig. 1. The coronal, sagittal, and axial views of the patient's CT scan images are extracted from CT scan images using Mimics software.

5. Grid independency

For the independency of the grid, five grids with sizes of 1.86, 2.63, 3.89, 4.85, 5.56, and 7.14 million tetrahedral elements were produced on the geometry. A pressure condition is considered for the outlets and the solution continues until convergence to the residual 10^{-4} (Fig. 2).

To compare the grids, the average shear stress was compared. The average shear stress in Fig. 3 in the section considered in the nasal cavity was compared for different grids. The difference at the end of the graphs is very small and economical, and therefore the grid of 3,897,064 elements is reliable and was used for the analysis.

6. Results and discussion

6.1. Particle absorption percentage

In this study, micrometer-sized particles are released from the nasal inlets into the respiratory tract. To solve the flow, drag, and gravity forces are considered, and after performing the analysis for particles with dimensions of 1, 2.5, and 10 μm in flow rates of 20, 25, and 30 which are laminar flow rates of 40, 60, and 100 which are turbulent flow, The percentage of particle precipitation is calculated using the equations given in the third chapter. In the results articles, the percentage of particle absorption is expressed as the horizontal axis in the graphs, instead of the particle diameter, the power of the two-particle diameters multiplied by the flow rate is used, which is called the impaction parameter (IP) [20]. Using this number, the graph of the percentage of particle absorption from the nasal inlet separately for laminar and turbulent flow is shown in Fig. 4 (a and b), respectively. The percentage of particle absorption for laminar flow and flow rates of 20, 25, and 30 lit/min is equal to 96.87 %, 97.19 %, and 97.64 %. With the increase of fluorite, the percentage of absorption of particles also increases.

The percentage of particle absorption for turbulent flow and flow rates of 40, 60, and 100 lit/min is equal to 98.67 %, 98.65 %, and 99.59 %. With the increase of fluorite, the percentage of absorption of particles also increases.

These figures show that the absorption of particles for 1, 2.5, and 10 μm is close to each other for quiet respiratory flows, while it does not show this in turbulent flow. As the diameter of the particles increases, the absorption of the particles increases so that the absorption in the nose for particles larger than 10 μm is more than 97 % and practically no more particles penetrate the lower part of the respiratory system and they are absorbed at the very beginning. Doctors and pharmacists with this information, i.e. the size of the particles and the place of deposition and the percentage of their absorption, and the correct selection of the entry of the particles into the respiratory system, can create sprays, medical devices, and appropriate drugs to improve respiratory patients as quickly as possible.

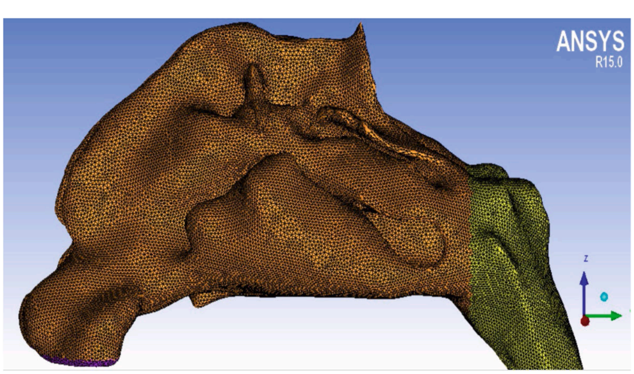

Fig. 2. Output model from Mimics software with STL extension including several thousand triangular elements.

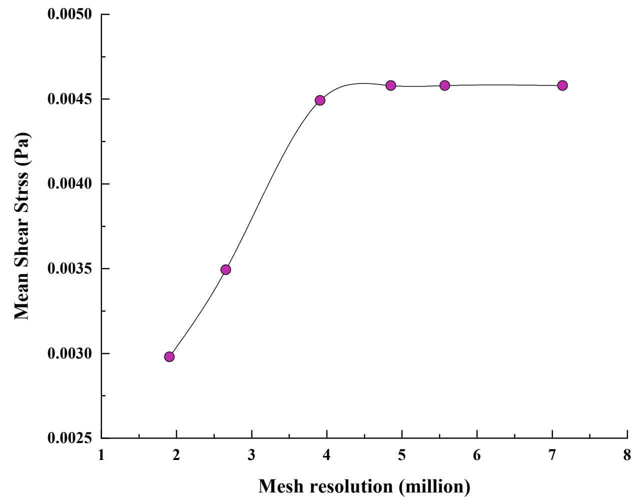

Fig. 3. Grid independency based on average shear stress.

6.2. Particle absorption percentage after wearing a respirator

After checking the airflow containing particles and absorbing them in the respiratory system, suppose we place a filter mask in front of the nose. Using the porous media tool, two respiratory filters with porosity of 0.2 and 0.07 were considered and checked at the entrance of the nostril. It should be noted that due to the very high computational volume, only the chamber or the left duct along with the nasopharynx, pharynx, larynx, and trachea were considered, and the right duct was not considered. Fig. 5 shows the deposition fraction as a function of the impaction parameter and flow rate for laminar flow, and turbulent flow with porosity 0.07. As you can see, the obtained results show that with the presence of a mask with a porosity of 0.07, the absorption of particles in the respiratory system is reduced. Numerically, for laminar flow with a flow rate of 20 lit/min, with increasing particle diameter, the percentage of particle absorption decreases from 1.12 % to 1 %. For a flow rate of 25 lit/min, with increasing particle diameter, the percentage of particle absorption decreases from 1.14 % to 1.02 %. For a flow rate of 30 lit/min, with increasing particle diameter, the percentage of particle absorption decreases from 1.34 % to 1.03 %. For turbulent flow with a flow rate of 40 lit/min, with increasing particle diameter, the percentage of particle absorption decreases from 1.29 % to 1.10 %. For a flow rate of 60 lit/min, with increasing particle diameter, the percentage of particle absorption decreases from 1.55 % to 1.20 %. For a flow rate of 100 lit/min, with increasing particle diameter, the percentage of particle absorption decreases from 1.64 % to 1.35 %.

Fig. 6 shows the deposition fraction as a function of the impaction parameter and flow rate for laminar flow, and turbulent flow with 0.2 porosity. As you can see, the obtained results show that with the presence of a mask with a porosity of 0.2 %, the absorption of particles in the respiratory system is reduced. Numerically, for laminar flow with a flow rate of 20 lit/min, with increasing particle diameter, the percentage of particle absorption decreases from 1.5 % to 1.20 %. For a flow rate of 25 lit/min, with increasing particle diameter, the percentage of particle absorption decreases from 1.64 % to 1.27 %. For a flow rate of 30 lit/min, with increasing particle diameter, the percentage of particle absorption decreases from 1.46 % to 1.16 %. For turbulent flow with a flow rate of 40 lit/min, with increasing particle diameter, the percentage of particle absorption decreases from 1.89 % to 1.43 %. For a flow rate of 60 lit/min, with increasing particle diameter, the percentage of particle absorption decreases from 1.94 % to 1.55 %. For a flow rate of 100 lit/min, with increasing particle diameter, the percentage of particle absorption decreases from 2.09 % to 1.63 %.

As it is known, with an increasing flow rate, more particles pass through the respiratory filter than with a lower flow rate. Based on these

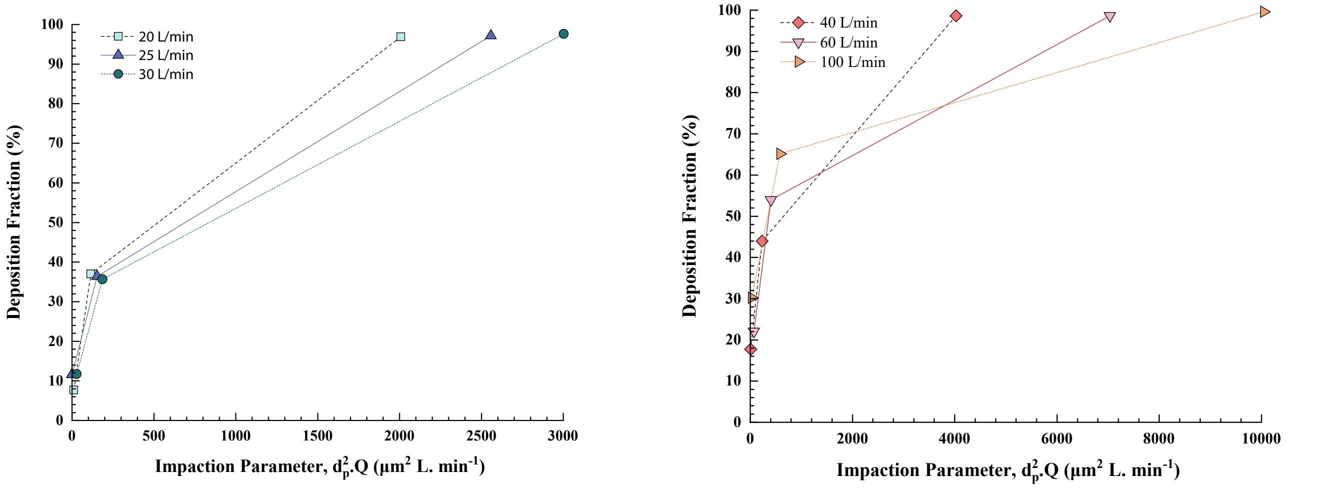

(a)

(b)

Fig. 4. The deposition fraction as a function of the impaction parameter and flow rate for (a) Laminar flow, and (b) Turbulent flow.

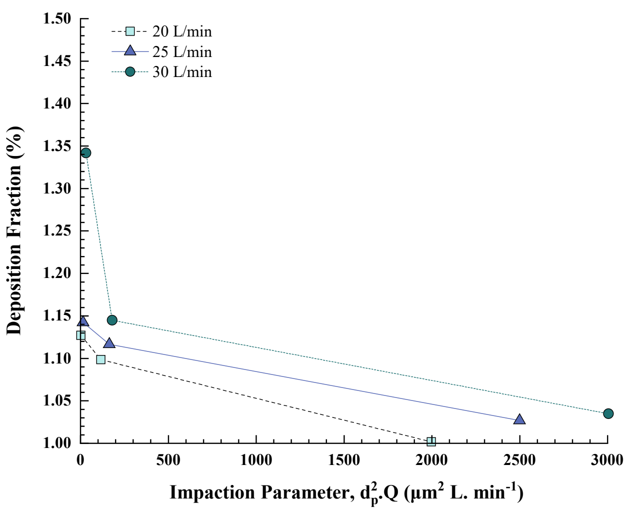

a) Laminar flow

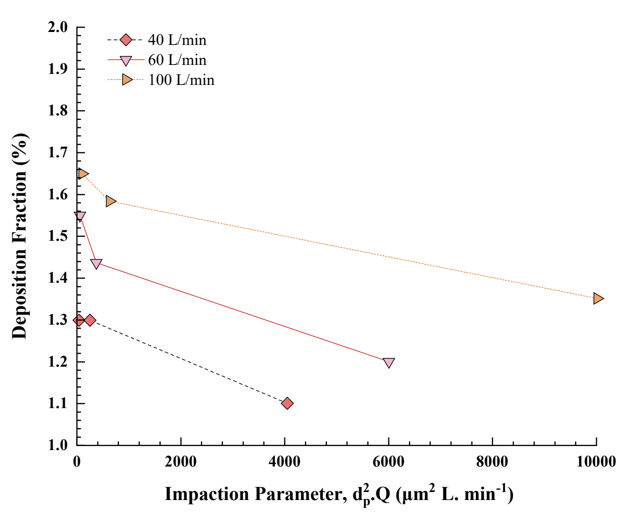

b) Turbulent flow

Fig. 5. The deposition fraction as a function of the impaction parameter and flow rate for (a) Laminar flow, and (b) Turbulent flow with porosity 0.07.

results in Figs. 5 and 6, it was found that the respiratory filter with a porosity of 0.07 is ideal and can filter particles up to 99 %. Most of the efforts of designers and manufacturers of filters are to absorb 1–2.5 μm, because most of the particles above 2.5 μm do not reach the lungs, and it is very difficult and expensive to filter particles below 1 μm. According to the results obtained in this project, in the porosity of 0.07, the filtration of 1-μm particles is the best compared to the rest of the investigated porosity.

7. Conclusion

PM or dust in the air is a type of pollution and one of the most important air pollutants in many areas. PM is made up of tiny solid particles or liquid droplets the size of a fraction of the thickness of human hair that float in the air we breathe. Breathing in contaminated particles can be harmful to your health. Larger particles called PM_{10} can irritate the eyes, nose, and throat. Dust from roads, fields, dry riverbeds, construction sites, and mines are types of PM_{10}. Smaller particles called $PM_{2.5}$ are more dangerous because they can get into the deeper parts of the lungs or even the blood. Particulate pollution can affect anyone, but it bothers some people more than others. In this research, the absorption of PM in the respiratory system was investigated. Then, using a porous environment, a breathing mask has been simulated and the absorption of particles after using the mask was checked, and the results obtained are as follows:

- The percentage of particle absorption for laminar flow and flow rates of 20, 25, and 30 lit/min is equal to 96.87 %, 97.19 %, and 97.64 %. With the increase of fluorite, the percentage of absorption of particles also increases.
- The percentage of particle absorption for turbulent flow and flow rates of 40, 60, and 100 lit/min is equal to 98.67 %, 98.65 %, and 99.59 %. With the increase of fluorite, the percentage of absorption of particles also increases.
- The absorption of particles for 1, 2.5, and 10 μm is close to each other for laminar respiratory flows, while it does not show this in a turbulent flow.
- For laminar flow and 0.07 porosity with a flow rate of 20 lit/min, with increasing particle diameter, the percentage of particle absorption decreases from 1.12 % to 1 %. For a flow rate of 25 lit/min, with increasing particle diameter, the percentage of particle absorption decreases from 1.14 % to 1.02 %. For a flow rate of 30 lit/min, with increasing particle diameter, the percentage of particle absorption decreases from 1.34 % to 1.03 %.

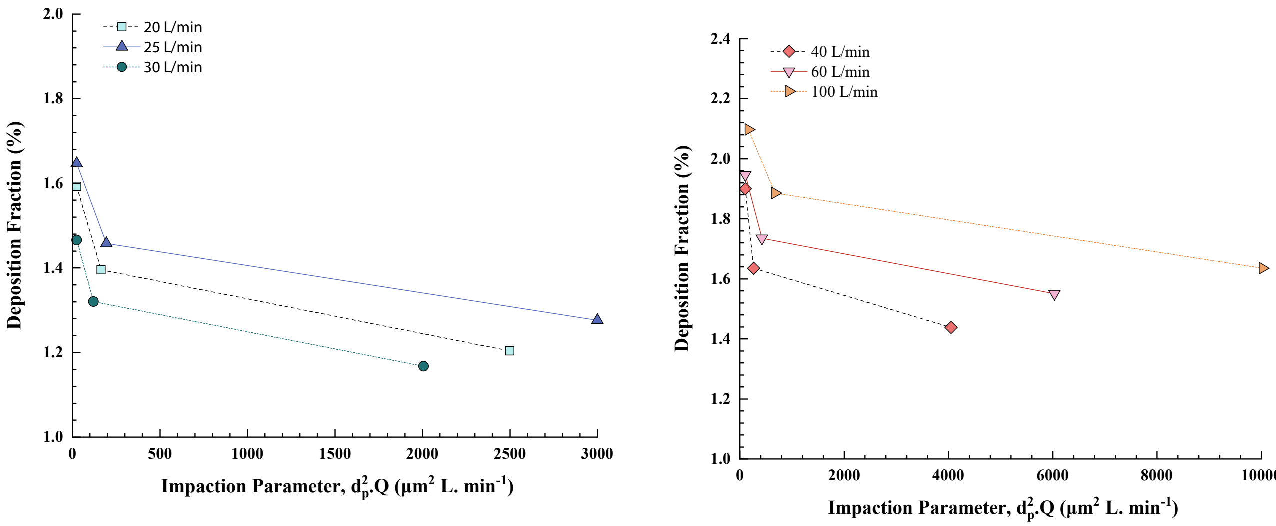

a) Laminar flow

b) Turbulent flow

Fig. 6. The deposition fraction as a function of the impaction parameter and flow rate for (a) Laminar flow, and (b) Turbulent flow with 0.2 porosity.

- For turbulent flow and 0.07 porosity with a flow rate of 40 lit/min, with increasing particle diameter, the percentage of particle absorption decreases from 1.29 % to 1.10 %. For a flow rate of 60 lit/min, with increasing particle diameter, the percentage of particle absorption decreases from 1.55 % to 1.20 %. For a flow rate of 100 lit/min, with increasing particle diameter, the percentage of particle absorption decreases from 1.64 % to 1.35 %.
- For laminar flow and 0.2 porosity with a flow rate of 20 lit/min, with increasing particle diameter, the percentage of particle absorption decreases from 1.5 % to 1.20 %. For a flow rate of 25 lit/min, with increasing particle diameter, the percentage of particle absorption decreases from 1.64 % to 1.27 %. For a flow rate of 30 lit/min, with increasing particle diameter, the percentage of particle absorption decreases from 1.46 % to 1.16 %.
- For turbulent flow and porosity 0.2 with a flow rate of 40 lit/min, with increasing particle diameter, the percentage of particle absorption decreases from 1.89 % to 1.43 %. For a flow rate of 60 lit/min, with increasing particle diameter, the percentage of particle absorption decreases from 1.94 % to 1.55 %. For a flow rate of 100 lit/min, with increasing particle diameter, the percentage of particle absorption decreases from 2.09 % to 1.63 %.

Declaration of Competing Interest

The authors declare that they have no known competing financial interests or personal relationships that could have appeared to influence the work reported in this paper.

References

[1] Zikirillo S, Ataboyev I. Air pollution and control engineering and technology. p. 155–9.
[2] Ban Y, Liu X, Yin Z, Li X, Yin L, Zheng W. Effect of urbanization on aerosol optical depth over Beijing: Land use and surface temperature analysis. Urban Climate 2023;51:101655. https://doi.org/10.1016/j.uclim.2023.101655.
[3] Laumbach RJ, Cromar KR. Personal interventions to reduce exposure to outdoor air pollution. Annu Rev Public Health 2022;43:293–309.
[4] Pritchett N, Spangler EC, Gray GM, Livinski AA, Sampson JN, Dawsey SM, et al. Exposure to outdoor particulate matter air pollution and risk of gastrointestinal cancers in adults: a systematic review and meta-analysis of epidemiologic evidence. Environ Health Perspect 2022;130(3):036001.
[5] Hu J, Li W, Gao Y, Zhao G, Jiang Y, Wang W, et al. Fine particulate matter air pollution and subclinical cardiovascular outcomes: a longitudinal study in 15 Chinese cities. Environ Int 2022;163:107218.
[6] Pryor JT, Cowley LO, Simonds SE. The physiological effects of air pollution: particulate matter, physiology and disease. Front Public Health 2022;10:882569.
[7] Garcia A, Santa-Helena E, De Falco A, de Paula Ribeiro J, Gioda A, Gioda CR. Toxicological effects of fine particulate matter (PM2.5): health risks and associated systemic injuries—systematic review. Water Air Soil Pollut 2023;234(6):346.
[8] Xu H, Jia Y, Sun Z, Su J, Liu QS, Zhou Q, et al. Environmental pollution, a hidden culprit for health issues. Eco-Environ Health 2022;1(1):31–45.
[9] Fazakas E, Neamtiu IA, Gurzau ES. Health effects of air pollutant mixtures (volatile organic compounds, particulate matter, sulfur and nitrogen oxides)–a review of the literature. Rev Environ Health 2023.
[10] Giacosa G, Rainham DG, Walker TR. A baseline characterization of fine particulate matter (PM2.5) concentration and releases in Nova Scotia, Canada. Atmosp Pollut Res 2023;14(5):101757.
[11] Flood-Garibay JA, Angulo-Molina A, Méndez-Rojas MÁ. Particulate matter and ultrafine particles in urban air pollution and their effect on the nervous system. Environ Sci Processes Impacts 2023;25(4):704–26.
[12] Kim Y-S, Kim H-G, Kwac L-K, Ko S-C. A study on the improvement of filter performance to remove indoor air pollution. Appl Sci 2023;13(4):2561.
[13] Nie W, Jiang C, Sun N, Guo L, Xue Q, Liu Q, et al. Analysis of multi-factor ventilation parameters for reducing energy air pollution in coal mines. Energy 2023;278:127732.
[14] Meesang W, Baothong E, Poojeera S, Kaenka W, Mathapha S, Srichat A, et al. Model feasibility of air pollution treatment using plants as filter by computational fluid dynamic (CFD) analysis: a case study in laboratory. Environ Asia 2022;15(1).
[15] McNabola A, Broderick B, Gill L. Reduced exposure to air pollution on the boardwalk in Dublin, Ireland. Measurement and prediction. Environ Int 2008;34(1):86–93.
[16] Langtry R, Menter F. Transition modeling for general CFD applications in aeronautics. p. 522.
[17] Ma B, Lutchen KR. CFD simulation of aerosol deposition in an anatomically based human large–medium airway model. Ann Biomed Eng 2009;37:271–85.
[18] Hinds WC, Zhu Y. Aerosol technology: properties, behavior, and measurement of airborne particles. John Wiley & Sons; 2022.
[19] Li A, Ahmadi G. Computer simulation of particle deposition in the upper tracheobronchial tree. Aerosol Sci Technol 1995;23(2):201–23.
[20] Cheng YS. Mechanisms of pharmaceutical aerosol deposition in the respiratory tract. AAPS PharmSciTech 2014;15:630–40.
[21] Khodabandeh E, Toghraie D, Chamkha A, Mashayekhi R, Akbari O, Rozati SA. Energy saving with using of elliptic pillows in turbulent flow of two-phase water-silver nanofluid in a spiral heat exchanger. Int J Numerical Method Heat & Fluid Flow 2020;30(4):2025–49. https://doi.org/10.1108/HFF-10-2018-0594.
[22] Pourdel H, Afrouzi HH, Akbari OA, et al. Numerical investigation of turbulent flow and heat transfer in flat tube. J Therm Anal Calorim 2019;135:3471–83. https://doi.org/10.1007/s10973-018-7529-8.
[23] Hosseinnezhad R, Akbari OA, Hassanzadeh H, et al. Numerical study of turbulent nanofluid heat transfer in a tubular heat exchanger with twin twisted-tape inserts. J Therm Anal Calorim 2018;132:741–59. https://doi.org/10.1007/s10973-017-6900-5.